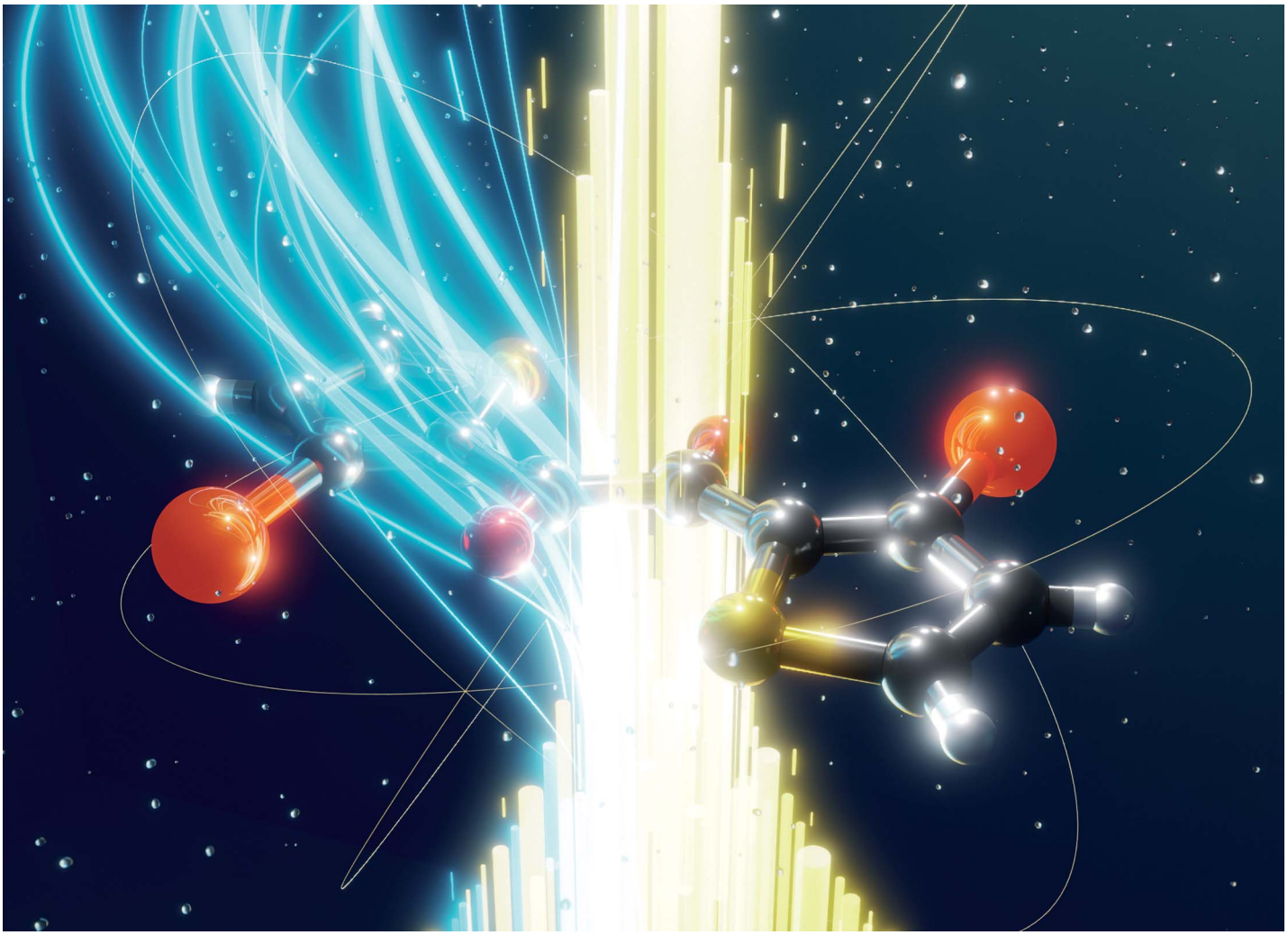

Showcasing research from Professor Tani's group, Department of Chemistry, Osaka University, Osaka, Japan, and Professor Miyata's group, Department of Chemistry, Kyushu University, Fukuoka, Japan.

Fast, efficient, narrowband room-temperature phosphorescence from metal-free 1,2-diketones: rational design and the mechanism

Fast room-temperature phosphorescence with high quantum yields up to 38% in solution from metal-free organic 1,2-diketones (the molecule in the image) are reported, along with the mechanism and molecular design principles governing the fast phosphorescence. This cover image depicts the key mechanism of the fast phosphorescence. The blue light rays come together into the molecule to generate bold yellow pillars, representing the acceleration of yellow phosphorescence through the mixing of high-lying singlet states.

As featured in:

See Yosuke Tani, Kiyoshi Miyata *et al.*, *Chem. Sci.*, 2024, **15**, 10784.

ROYAL SOCIETY OF CHEMISTRY

rsc.li/chemical-science

Registered charity number: 207890

Chemical Science

ROYAL SOCIETY OF CHEMISTRY

EDGE ARTICLE

View Article Online
View Journal | View Issue

Cite this: *Chem. Sci.*, 2024, **15**, 10784

All publication charges for this article have been paid for by the Royal Society of Chemistry

Fast, efficient, narrowband room-temperature phosphorescence from metal-free 1,2-diketones: rational design and the mechanism†

Yosuke Tani, *[ab] Kiyoshi Miyata, *[c] Erika Ou,[a] Yuya Oshima,[a] Mao Komura,[a] Morihisa Terasaki,[a] Shuji Kimura,[c] Takumi Ehara,[c] Koki Kubo,[c] Ken Onda[c] and Takuji Ogawa[a]

We report metal-free organic 1,2-diketones that exhibit fast and highly efficient room-temperature phosphorescence (RTP) with high colour purity under various conditions, including solutions. RTP quantum yields reached 38.2% in solution under Ar, 54% in a polymer matrix in air, and 50% in crystalline solids in air. Moreover, the narrowband RTP consistently dominated the steady-state emission, regardless of the molecular environment. Detailed mechanistic studies using ultrafast spectroscopy, single-crystal X-ray structure analysis, and theoretical calculations revealed picosecond intersystem crossing (ISC) followed by RTP from a planar conformation. Notably, the phosphorescence rate constant k_p was unambiguously established as ~5000 s^{-1}, which is comparable to that of platinum porphyrins (representative heavy-metal phosphor). This inherently large k_p enabled the high-efficiency RTP across diverse molecular environments, thus complementing the streamlined persistent RTP approach. The mechanism behind the photofunction has been elucidated as follows: (1) the large k_p is due to efficient intensity borrowing of the T_1 state from the bright S_3 state, (2) the rapid ISC occurs from the S_1 to the T_3 state because these states are nearly isoenergetic and have a considerable spin–orbit coupling, and (3) the narrowband emission results from the minimal geometry change between the T_1 and S_0 states. Such mechanistic understanding based on molecular orbitals, as well as the structure-RTP property relationship study, highlighted design principles embodied by the diketone planar conformer. The fast RTP strategy enables development of organic phosphors with emissions independent of environmental conditions, thereby offering alternatives to precious-metal based phosphors.

Received 29th April 2024
Accepted 1st June 2024

DOI: 10.1039/d4sc02841d

rsc.li/chemical-science

Introduction

Room-temperature phosphorescence (RTP) from metal-free organic molecules has been an area of intense research.[1] Although classical RTP materials have been used for diverse applications, including organic light-emitting diodes (OLEDs) and bioimaging, they are mainly precious-metal complexes of Ir or Pt.[2] Therefore, cost-effective, less-toxic, and sustainable metal-free alternatives are needed. However, intrinsic molecular RTP of metal-free phosphors has not rivalled that of metal complexes.

Organic RTP must overcome several challenges stemming from the absence of heavy-metal atoms. The most severe is the inherently small phosphorescence transition probability (*i.e.*, rate constant k_p), causing poor RTP quantum yields (Φ_p). k_p can be 10^4–10^5 s^{-1} for heavy-metal complexes,[3] and only ~10 s^{-1} or less for conventional organic compounds.[1a] Introducing heavy atoms, such as bromine, iodine, selenium, and tellurium, in conjunction with carbonyl functionalities, is a classical approach for enhancing k_p.[4] Despite its long history, however, an organic k_p over ~100 s^{-1} and/or a Φ_p over 1% in solutions are rarely observed (Fig. 1b, blue filled circles; Fig. S1 and Table S1†).[5] The use of thiocarbonyls could provide a large k_p in some cases (Fig. 1b, blue open circles).[6] However, they are associated with high (photo)chemical reactivities and instability,[7] thereby limiting their high Φ_p in perfluoroalkane solvents.[6b] The only practical way to improve Φ_p has been to reduce the nonradiative decay rate constant (k_{nr}). This approach has provided solid-state phosphors with RTP lasting for subseconds after excitation cessation (persistent RTP or afterglow).[8] However, it inevitably

[a]*Department of Chemistry, Graduate School of Science, Osaka University, Machikaneyama 1-1, Toyonaka, Osaka 560-0043, Japan. E-mail: y-tani@chem.sci.osaka-u.ac.jp*

[b]*Innovative Catalysis Science Division, Institute for Open and Transdisciplinary Research Initiatives (ICS-OTRI), Osaka University, Suita, Osaka 560-8531, Japan*

[c]*Department of Chemistry, Faculty of Science, Kyushu University, 744 Motooka, Nishi, Fukuoka 819-0395, Japan. E-mail: kmiyata@chem.kyushu-univ.jp*

† Electronic supplementary information (ESI) available: Experimental procedures, analytical data, physicochemical properties, computational details, and CIF files for the single-crystal X-ray structure analysis. CCDC 2269866. For ESI and crystallographic data in CIF or other electronic format see DOI: https://doi.org/10.1039/d4sc02841d

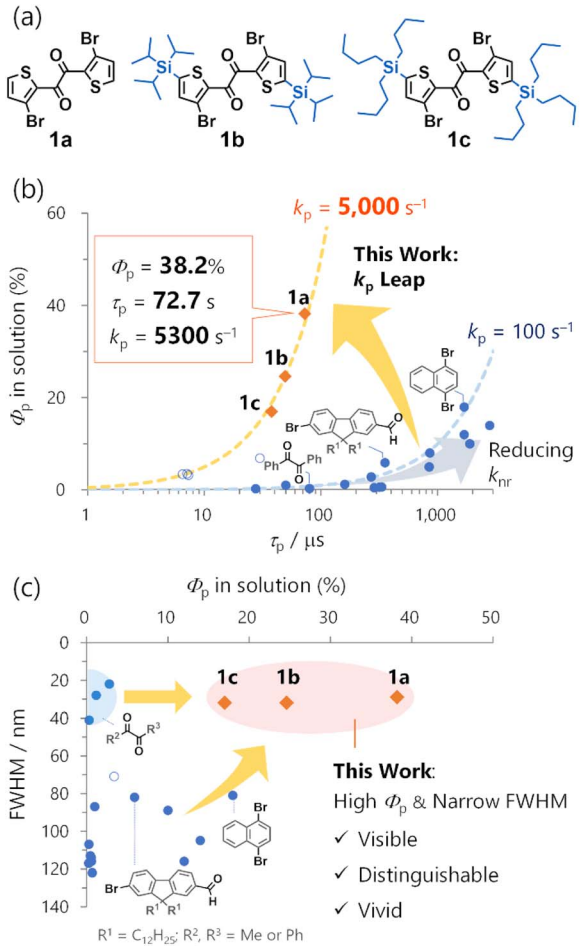

Fig. 1 Comparison of representative metal-free organic phosphors (blue filled circles), thiocarbonyls (blue open circles), and **1** (orange diamonds) in solution. (a) Molecular structures of **1**. (b) Room-temperature phosphorescence quantum yields (Φ_p) *vs.* lifetimes (τ_p); (c) full-width-at-half-maxima (FWHM) *vs.* Φ_p. Blue and orange broken lines in (b) represent k_p = 100 and 5000 s^{-1}, respectively, assuming unity intersystem crossing quantum yields.

restricts the organic phosphors to rigid media, such as crystals,[9] or tailored host–guest systems with strong intermolecular interactions.[10]

A promising direction for environmentally independent organic RTP could be the significant increase in k_ps. Complementary to the persistent RTP, fast RTP could have significant potential use in solutions or any non-rigid molecular environment, including biological conditions.[11] Moreover, because fast RTP can avoid efficiency loss caused by the accumulation of the triplet excitons, it also could be used in optoelectronics such as OLEDs.[12] However, the quest for fast RTP is facing difficulty so far. In 2022, a selenium-containing molecule (phenoxaselenine) was designed as a candidate for fast RTP; however, its RTP was weak even in a polymer matrix, and only the photoluminescence spectrum and intrinsic phosphorescence rate (*ca.* 4000 s^{-1}) at 78 K were reported.[13] Quite recently, organic ionic crystals were reported to exhibit fast RTP with impressive k_p values up to ~10^5 s^{-1}.[14] The authors ascribed the large k_p to the external heavy atom effect of two appropriately arranged iodide counter anions. Nonetheless, such effects relied on the crystal packing, and no RTP was observed in solutions. Thus, molecular design for a large k_p that enables RTP in solution is needed.

Low colour purity is another organic RTP challenge. Considering the luminescence of the same quantum efficiency, high-colour-purity emission has a sharp and intense spectral peak that is visible, distinguishable, and vivid. These are essential features for OLED displays and bioimaging.[15] However, organic RTP is usually broad with 80–120 nm full-width at half-maxima (FWHMs) (Fig. 1b, Table S1†). Moreover, because of an inefficient intersystem crossing (ISC) from singlet to triplet states, organic phosphors often exhibit both RTP and fluorescence, further impairing colour purity. As a long-known exception, 1,2-diketones, such as biacetyl and benzil, exhibit narrowband RTP that consists of one main peak with a small FWHM value accompanied by weak vibronic bands.[16] However, the RTP is feeble in solution. Thus, simultaneously achieving a high Φ_p and colour purity in organic RTP remains a tremendous challenge.

Using heteroaromatic 1,2-diketones, we previously developed a series of solid-state mechanoresponsive RTP materials,[17] solvent-free liquid RTP materials,[18] and photoresponsive RTP crystals (Fig. S3†).[19] They exhibited RTP in non-rigid molecular environments, such as amorphous solids or solvent-free liquids, wherein conventional metal-free organic compounds rarely show RTP. Thus, our previous results not only demonstrated unique advantages of the 1,2-diketone-based materials in applications, but also implied large k_ps. However, the fundamental molecular RTP properties remain elusive due to the complexity of the condensed materials. While we have briefly reported some solution-phase RTP properties of thienyl diketones **1a** and **1b**,[17a] further investigations were necessary to evaluate k_p quantitatively (Fig. 1a and S2†). Typically, k_p is derived from experimental Φ_p, ISC quantum yield ϕ_{ISC}, and RTP lifetime τ_p, expressed as $k_p = \Phi_p/(\phi_{ISC} \times \tau_p)$. However, ϕ_{ISC} was not evaluated in our prior research as we did not focus on k_p. In addition, while we determined Φ_p and τ_p of **1b**, the previous protocol did not assure consistent degassing for those measurements (*i.e.*, the extent of oxygen quenching of RTP would be different; Fig. S2†). Consequently, these values cannot be employed to establish k_p. Therefore, the mechanism governing the expected fast RTP remained unexplored, not to mention the absence of the molecular design principle for substantial k_p.

Here, we disclose the inherent molecular RTP properties of the thienyl diketone derivatives **1**, exhibiting high-efficiency narrowband RTP based on an exceptionally large k_ps of ~5000 s^{-1} (Fig. 1). In particular, **1a** exhibited 38.2% Φ_p in cyclohexane. To our knowledge, this is the highest efficiency for metal-free organic molecules in common solvents. Relative to benzil, the k_p was increased by a factor of ~100 from 39 s^{-1} to 5300 s^{-1}, enabling a 100-time increase in Φ_p from 0.31% to 38% (Fig. 1a).[16c] Moreover, high Φ_p with a narrow ~30 nm FWHM was observed in solution (Fig. 1b). The high efficiency and colour purity were also observed in various conventional polymer matrices and crystalline solids, indicating that the RTP was

an inherent molecular feature. The RTP mechanism and origin were revealed through single-crystal X-ray structure analysis, time-resolved photoluminescence (TRPL) spectroscopy, transient absorption (TA) spectroscopy, time-resolved infrared (TRIR) spectroscopy, and quantum-chemical calculations. Furthermore, structure-RTP property relationship study considering molecular- and natural transition orbitals provided design principles for fast organic RTP. Our work demonstrates the potential of metal-free organic molecular materials to exhibit fast RTP comparable to precious-metal complexes. Complementary to persistent RTP, organic fast RTP is promising not only for application in solution but also in functional condensed materials as we have witnessed in our previous studies (Fig. S3†).

Results and discussion

RTP and related rate constants of 1a

We first examined the RTP properties in solution for the diketone **1a**, which exhibits strong yellow emission (Fig. 2a and b). The steady-state photoluminescence spectrum of **1a** in cyclohexane had a single, sharp emission peak at 560 nm accompanied by weak vibronic bands at 615 and ~680 nm.[20] The total photoluminescence quantum yield Φ_{PL} was 38.2% under Ar and the lifetime was 72.7 μs, as determined with a protocol that assures consistent degassing for both measurements (Scheme S2†). TRPL spectra of **1a** revealed that the emission emerged just after photoexcitation (within a <100 ps instrumental response function), and exhibited a long lifetime (Fig. S11†). Hence, the emission was phosphorescence, as reported previously for thienyl diketone analogs,[17] and ISC occurred over a timescale less than the instrumental response.

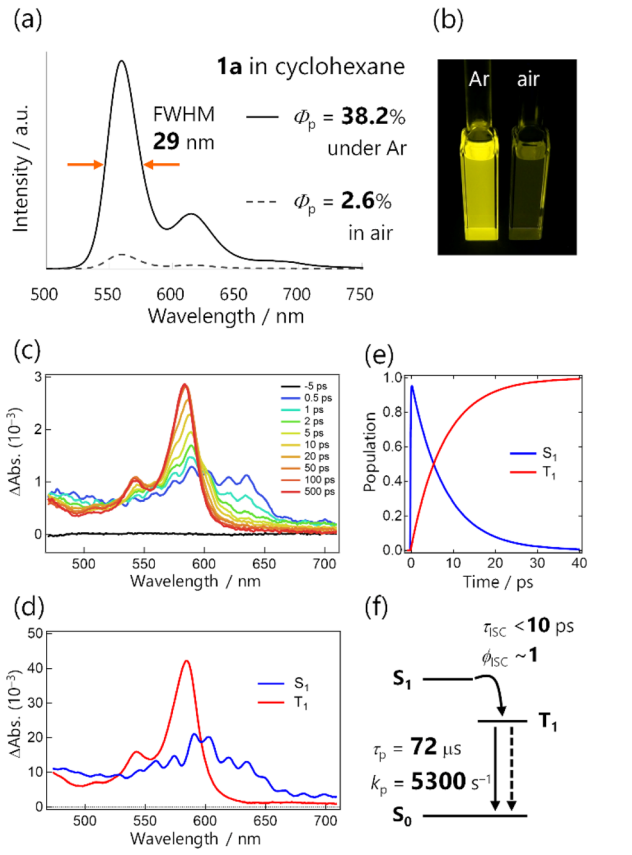

Fig. 2 (a) Steady-state photoluminescence spectra of **1a** in cyclohexane (4.4×10^{-6} M, excited at 368 nm). (b) Photograph of solutions under 365 nm excitation. (c) fs transient absorption spectra of **1a** in cyclohexane excited at 355 nm. (d and e) Selected results from the global analysis based on a sequential model; (d) evolution-associated spectra and (e) corresponding concentration kinetics. Coherent artefact signals are omitted for clarity. (f) Schematic summary of the excited-state dynamics in **1a**.

To quantify the rapid ISC, we conducted femtosecond TA spectrum (fsTAS) measurement with ~100 fs time resolution (Fig. 2c). The broad transient absorption over 450–650 nm changed to sharp spectra with a peak at 580 nm in a ~10 ps timescale. We globally analysed the TAS by using a sequential model assuming two excited species, resulting in successful fitting with the time constant of the transition estimated to be 7.9 ps (Fig. 2d and e and S14†). We also conducted TAS measurements over nanosecond timescales (Fig. S13†), and observed that the TAS shape was unchanged up to the microsecond timescale. The long-lived spectral component was the lowest triplet excited state (T_1 state), populated *via* ISC with a time constant of <10 ps for **1a** in solution (Fig. 2f). Because the ISC outcompeted other relaxation processes, we can reasonably assume that the ISC quantum yield (ϕ_{ISC}) was unity.

The total photoluminescence quantum yield can be expressed as $\Phi_{PL} = \Phi_f + \Phi_p$, where Φ_f is the fluorescence quantum yield. Given that $\phi_{ISC} \sim 1$, phosphorescence dominates the total emission, and $\Phi_p \sim \Phi_{PL} = 0.38$. To the best of our knowledge,[21–23] this is a record-breaking RTP efficiency for metal-free organic molecules in common solvents. In addition, with $\phi_{ISC} \sim 1$ confirmed, $\Phi_p = \phi_{ISC} k_p \tau_p \sim k_p \tau_p$. For $\Phi_p = 0.38$ and $\tau_p = 72.7$ μs, k_p was derived to be 5300 s^{-1}, which greatly exceeded those of previously reported organic phosphors, except for thiocarbonyl compounds (Fig. 1a and Table S1†). Because of this exceptionally high k_p, the RTP of **1a** in solution was visible even in air (Φ_p = 2.6%, Fig. 2a and b, S10, Table S2, and ESI Movie 1†). We note that the estimation of k_p in the literature often assumed $\phi_{ISC} = 1$ and $\Phi_p \sim \Phi_{PL}$ without evaluating the time constant of ISC, and employed Φ_p and τ_p that were determined without assuring consistent degassing. This would be practical for qualitative purposes, but may cause significant errors in the k_p value. Experimental evaluation of ϕ_{ISC} and assuring consistent degassing are essential for the quantitative evaluation of k_p.

The emission colour purity is also outstanding. Fluorescence was not discernible in the steady-state photoluminescence, and the FWHM of the RTP was only 29 nm for **1a** (Fig. 2a and S10†). The RTP contained two other vibronic bands at around 615 and 680 nm; nonetheless, the first band at 560 nm covered 71% of the whole spectral area (Table S3†). This is distinct from other organic phosphors, which have broad and structure-less spectra with a 80–120 nm FWHM (Fig. 1c and Table S1†). Although there is a room for further improvement, the narrowband RTP with weak vibronic bands and the fluorescence-free nature represented a high colour purity emission; its coordinates (0.45,

0.54) are located almost at the edge of the chromaticity diagram of Commission internationale de l'éclairage (CIE) 1931 (Fig. 3b).

Substituent effect

Next, we investigated the effects of trialkylsilyl substituents on the RTP properties in solution. Trialkylsilyl substituents are known to perturb π-electronic systems through σ–π and/or σ*–π* conjugation (hyperconjugation). While these substituents sometimes improve the fluorescence efficiency, their effects on RTP properties have gained less attention.[9d,24]

We introduced triisopropylsilyl (**1b**) and tributylsilyl groups (**1c**) onto the thienyl diketone core (Fig. 1a) and examined their properties in cyclohexane solution. The silylated derivatives **1b** and **1c** provided identical emission spectra with the maxima slightly red-shifted from 560 nm to 568 nm compared to those of **1a** (Fig. 3a and S10†). The steady-state emissions were fluorescence-free and maintained a small FWHM (32 nm). This narrowband yellow emission had a CIE 1931 coordinate of (0.49, 051) (Fig. 3b).[2c] We also conducted fsTAS measurement for **1b** (Fig. S15†) to analyse ISC; the main feature of the TAS was largely the same as that for **1a** and the ISC time constants were 0.63 and 2.3 ps. The time constant is even faster than that of **1a** and we can assume unity ϕ_{ISC} for the silylated diketones. Φ_p for **1b** and **1c** was less than that for **1a**, but still 24.6 and 17%, respectively (Fig. 3c). The decrease in Φ_p could be attributed to the doubled k_{nr} values, from 8500 s^{-1} for **1a** to 15000 s^{-1} and 22000 s^{-1} for **1b** and **1c**, respectively. This was most likely because of the nonradiative decay accelerated by molecular motion involving the silyl groups. In contrast, k_p values were only slightly changed, 5000 and 4500 s^{-1} for **1b** and **1c**. These results indicated that the large k_p of **1** basically originated from the thienyl diketone core.

RTP of 1-doped polymer films in air

The huge k_p of **1** enabled efficient RTP in air in the amorphous state using various conventional polymers as matrices (Fig. 3d–f and S20–S24 and Table S4†). The best Φ_p of 54% was achieved at room temperature in air for a poly(methyl methacrylate)

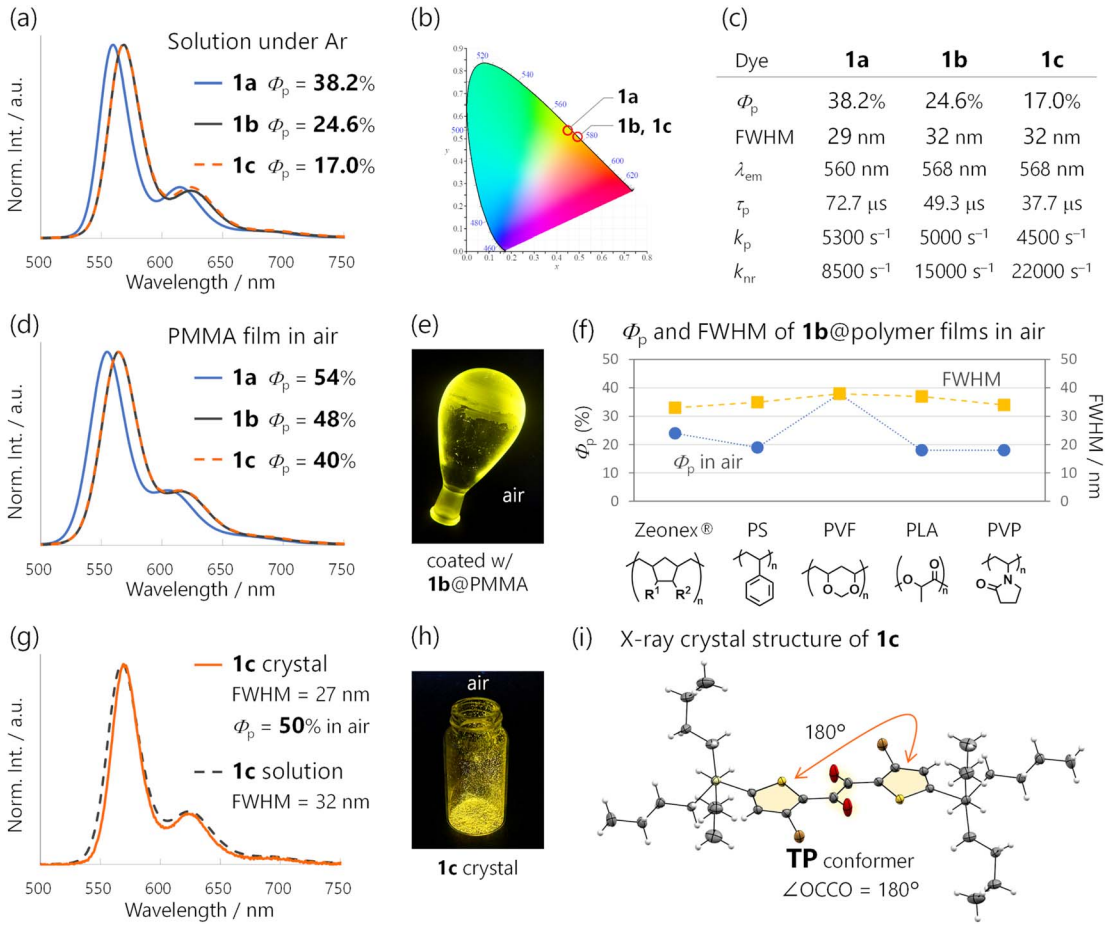

Fig. 3 (a) Steady-state photoluminescence (PL) spectra of **1a–1c** in cyclohexane ($10–4.4 \times 10^{-6}$ M, excited at 368 nm) and (b) CIE1931 chromaticity diagram for their PL in cyclohexane. (c) Photophysical properties of **1a–1c** in cyclohexane under Ar ($10–4.4 \times 10^{-6}$ M, excited at 368 nm). Φ_p, RTP quantum yields; FWHM, full-width-at-half-maxima; λ_{em}, emission maxima; τ_p, lifetimes; k_p and k_{nr}, phosphorescence and non-radiative rate constants. (d and g) Steady-state PL spectra of (d) **1a–1c**@PMMA (5 wt%, excited at 355–368 nm) and (g) a **1c** crystal in cyclohexane (1.0×10^{-5} M, excited at 368 nm). (e and h) Photographs of (e) **1b**@PMMA and (h) a **1c** crystal under 365 nm excitation. (f) Φ_p in air and the FWHM of **1b**-doped polymer films (5 wt%, excited at 350–375 nm). (i) ORTEP drawing of the crystal structure of **1c**. Thermal ellipsoids are set at the 50% probability level.

(PMMA) film doped with 5-wt% **1a** (Fig. 3d). The PMMA films doped with silylated diketones **1b** and **1c** also provided narrowband PL spectra similar to that of **1a** and exhibited a high Φ_p of 48 and 40%, respectively (Fig. 3d and e). These were among the highest reported for polymer-based RTP systems doped with metal-free organic dyes.[25] The reported systems with insufficient k_p required a tailor-made approach that involves specific interactions between the polymers and dopants. Hydrogen bonding in poly(vinyl alcohol) was reported to be effective and widely used,[10c–e] but these interactions or polymers are difficult to use under highly humid conditions or in water. Because PMMA is resistant to water, the RTP properties of a **1c**-doped PMMA film were not spoiled by water, exhibiting the same PL spectrum with a Φ_p of 35% even when submerged in water (Fig. S22†).[26]

Moreover, phosphorescent films with Φ_p values of 38–18% were obtained by doping **1b** into other five conventional polymers (Fig. 3f and S23, S24 and Table S4†). The emission maxima and FWHMs were almost unchanged, with colour purities independent of the polymers. Thus, RTP properties of the films were derived from inherent characteristics of **1**.

We would like to emphasize that achieving efficient organic RTP in solution and in polymer matrices is challenging because nonradiative decay is not suppressed under these conditions. In such cases, the fast RTP (large k_p) has a distinct advantage over persistent RTP with small k_p. The same can be said for the RTP in non-crystalline aggregate states, such as the amorphous solid state and solvent-free liquid state. It becomes clear that our previous studies of mechanoresponsive RTP materials,[17] solvent-free liquid RTP materials,[18] and photoresponsive RTP crystals[19] (Fig. S3†) demonstrated the usefulness and applications of fast RTP.

Conformation of RTP-emitting species

Considering that **1** has three successive single bonds in the diketone core, identifying the RTP-emitting conformation was important.[16b–d,27] In our previous study, two distinct conformers of thienyl diketones were identified by single-crystal X-ray structure analysis.[17a] The **1a** crystal exhibited a *trans*-planar (TP) conformation with respect to the dicarbonyl moiety, while the **1b** crystal exhibited a skew conformation (Fig. S33†). Thus, the conformation in crystals varied based on the substituents due to subtle differences in the intermolecular interactions. Unfortunately, the **1a** crystal was nonemissive, likely due to intermolecular electronic interactions. **1a** exhibited one-dimensional columnar π-stacking with a 3.481 Å interplanar distance, and the absorption of the crystal had a long tail until over 700 nm (Fig. S34†). On the other hand, the **1b** crystal emitted green RTP, which was different from the solution RTP. Therefore, further study was required to nail down the conformation of the yellow RTP-emitting species.

In the present work, we found that crystals of **1c** exhibited yellow RTP with a 50% Φ_p in air (Fig. 3g and h). The RTP decayed as a single exponential with a τ_p of 79 μs, and k_p was 6000 s^{-1} (Fig. S25†). Most importantly, the PL spectrum was almost identical to that of **1c** in solution, indicating emission from the same conformer (Fig. 3g). Single-crystal X-ray structure analysis revealed the TP conformation of **1c**, with the thienyl diketone core spatially separated from neighbouring molecules by tributylsilyl substituents (Fig. 3i and S32†; no π-stacking, and the interplanar distance was 4.45 Å). Thus, the RTP from the **1c** crystal, as well as **1** in solution, was unambiguously assigned to the monomer emission from its TP conformer. Notably, **1c** represents a rare example of metal-free organic molecules exhibiting remarkable Φ_p in solution, in a polymer matrix, and in a crystal, with almost identical PL spectra.

To experimentally elucidate conformation dynamics in the excited state, TRIR spectroscopy was performed. Although we could not perform the TRIR measurement on **1a** because of poor solubility, we managed to conduct the TRIR measurement on **1b** in cyclohexane using a 267 nm wavelength pump light (Fig. S16†). The spectra converged to sharp spectra over 0.74 ps and 2.67 ps timescales, consistent with the time constants extracted from fsTAS of **1b** (0.63 and 2.3 ps, Fig. S15†). Note that these time constants were comparable to those observed for **1a** in the fsTAS measurement. This indicated that the excited-state dynamics were primarily affected by the thienyl diketone core, while the silyl groups had minor effects. The two timescales were attributed to the conformation change and ISC. More importantly, the converged TRIR spectra were consistent with simulated spectra, assuming a TP conformation in the T_1 state (Fig. S17†). Thus, both the conformation changes and the ISC were ultrafast, and the RTP is confirmed to originate from the TP conformer.

Origin of the rapid ISC

Given that the ISC occurs at the TP conformation, we investigated the molecular origin of the rapid ISC by time-dependent density functional theory (TDDFT) calculations (Fig. 4 and S26†). In principle, ISC is fast when the energy gap is small and the spin–orbit coupling (SOC) matrix element is large.[28] In the S_1-optimized TP geometry, the S_1 state was almost isoenergetic to the T_3 state (energy gap <0.01 eV for **1a** and 0.04 eV for **1b** at the TDA/uCAM-B3LYP-D3/6-311G(d) level of theory).[29] Moreover, the S_1–T_3 SOC matrix elements $\langle S_1|\mathbf{H}_{SO}|T_3\rangle$ for **1a** and **1b**

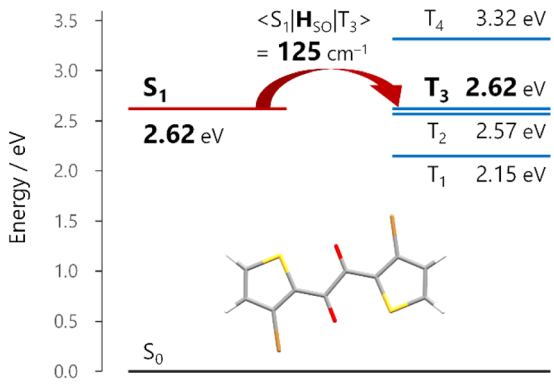

Fig. 4 Energy diagram of **1a** in the S_1-optimized *trans*-planar (TP) geometry. Energies and the spin–orbit coupling matrix element between the S_1 and T_3 states $\langle S_1|\mathbf{H}_{SO}|T_3\rangle$ were calculated at the TDA/uCAM-B3LYP-D3/6-311G(d) level of theory.

were 125 and 112 cm^{-1}, respectively. The substantial SOC matrix elements were consistent with El Sayed's rule; the electronic configurations of the S_1 and T_3 states were (n,π*) and (π,π*), respectively (Fig. S26†). These results strongly supported the ultrafast ISC, which occurred dominantly from the S_1 to T_3 states, followed by internal conversion to the T_1 state.

Origin of the substantial k_p value

Based on concrete basis that the RTP comes from the TP conformer, we then investigated the origin of the outstanding k_p. Theoretically, it was roughly based on intensity borrowing from the *n*th excited singlet states (S_n), as given by:[28a]

$$k_p \propto (\Delta E_{T_1-S_0})^3 |M_p|^2 \quad (1)$$

$$M_p = \sum_n m_p{}^n \quad (2)$$

$$m_p{}^n = \mu_{S_n-S_0} \frac{\langle S_n|H_{SO}|T_1\rangle}{\Delta E_{S_n-T_1}} \quad (3)$$

where M_p and $\mu_{S_n-S_0}$ are the T_1–S_0 and S_n–S_0 transition dipole moments at the T_1-geometry, respectively; $m_p{}^n$ contributed to M_p by borrowing intensity from the S_n state; $\langle S_n|H_{SO}|T_1\rangle$ is the SOC matrix element between the S_n and T_1 states. Eqn (1)–(3) provide two insights: (i) $m_p{}^n$, and hence k_p, increase when S_n states of a large (spin-allowed) $\mu_{S_n-S_0}$ couple with the T_1 state; and (ii) the coupling increases when SOC with energetically close S_n states is effective; $\langle S_n|H_{SO}|T_1\rangle/\Delta E_{S_n-T_1}$ can be regarded as the mixing coefficient. It should be emphasized that a large SOC matrix element is insufficient because matching of the three factors in eqn (3) *via* the same S_n states is the requisite for a significant k_p.

TDDFT calculations for the T_1-optimized TP geometry of **1a** yielded $k_p = 5400\ s^{-1}$ (for $n = 1$–6), which excellently reproduced the experimental value of 5300 s^{-1}. Remarkably, the T_1 state strongly coupled with the S_3 state (Fig. 5a); a large SOC matrix element $\langle S_3|H_{SO}|T_1\rangle = 167\ cm^{-1}$ and a reasonable $\Delta E_{S_3-T_1} = 1.74$ eV $= 14\,000\ cm^{-1}$ provided a large mixing coefficient $\langle S_3|H_{SO}|T_1\rangle/\Delta E_{S_3-T_1}$ of 1.19×10^{-2}. This coefficient indicates that the T_1 state can borrow 1.19% of the transition dipole moment between the S_3 and S_0 states (*i.e.*, $\mu_{S_3-S_0}$), which is quite large for phosphorescence. Furthermore, the $|\mu_{S_3-S_0}|$ was as large as 4.68 *D*, thus realizing a large $|m_p{}^3| = 56 \times 10^{-3}$ *D*. The contribution from $m_p{}^3$ corresponded to 93% of the total k_p value and is obviously the source of the large k_p (Fig. 6b, *vide infra*). Similar results were obtained for **1b**, confirming that the origin of the substantial k_p lies in the thienyl diketone core (Table S5†).

The natural transition orbitals (NTOs) of the S_3 and T_1 states provided an intuitive understanding of the large $\mu_{S_3-S_0}$ and $\langle S_3|H_{SO}|T_1\rangle$ (Fig. 5b). First, the S_3 state (S_3–S_0 transition) had a pure (π,π*) configuration, where the NTOs delocalized over the entire molecule in a planar geometry, which was favourable for large μ. On the other hand, the T_1 state had a pure (n,π*) configuration, *i.e.*, it was not contaminated with (π,π*) character. The pure ^{3}(n,π*) configuration enabled SOC with the pure ^{1}(π,π*) state, consistent with El Sayed's rule.[4a] The pure (n,π*)/(π,π*) characters are noteworthy, because excited states with mixed (n,π*) and (π,π*) configurations diminish SOC.[30] Most importantly, the hole NTOs of the S_3 and T_1 states around the heavy atoms, especially Br, were mutually perpendicular. This is ideal because the spin–orbit Hamiltonian H_{SO} involves the orbital angular-momentum operator that rotates the orbitals by 90°.[13,28a] Thus, for the hole-constituting atomic orbital of Br, the in-plane σ-symmetric n orbital of T_1 states (Fig. 5b bottom-right) became π-symmetric, producing a significant spatial integral with the out-of-plane p orbital of the S_3 state (Fig. 5b bottom-left). The large spatial integral near the heavy nuclei boosts the heavy-atom effect, resulting in a large $\langle S_3|H_{SO}|T_1\rangle = 167\ cm^{-1}$. Thus, **1** embodies an ideal electronic structure for intensity-borrowing that enhances k_p: (1) a planar π-system that produces large μ; (2) carbonyl groups in the π-plane that joined the pure ^{1}(π,π*) and pure ^{3}(n,π*) states; and (3) heavy atoms with electrons conjugated to both the π and σ-/n-systems to boost $\langle S_n|H_{SO}|T_1\rangle$.

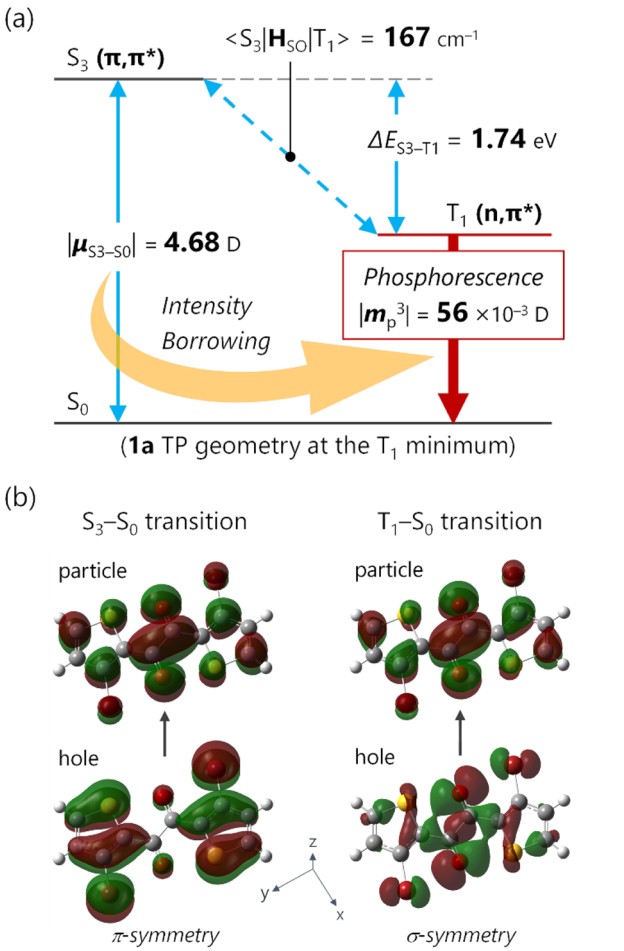

Fig. 5 (a) Energy diagram of **1a** in the T_1-optimized *trans*-planar (TP) geometry depicting the principal intensity-borrowing. Energies, the transition dipole moment $\mu_{S_3-S_0}$, and the spin–orbit coupling matrix element $\langle S_3|H_{SO}|T_1\rangle$ were calculated at the TDA/(u)CAM-B3LYP-D3/6-311G(d) level. (b) Principal natural transition orbitals (NTOs) for S_3–S_0 (left) and T_1–S_0 (right) transitions.

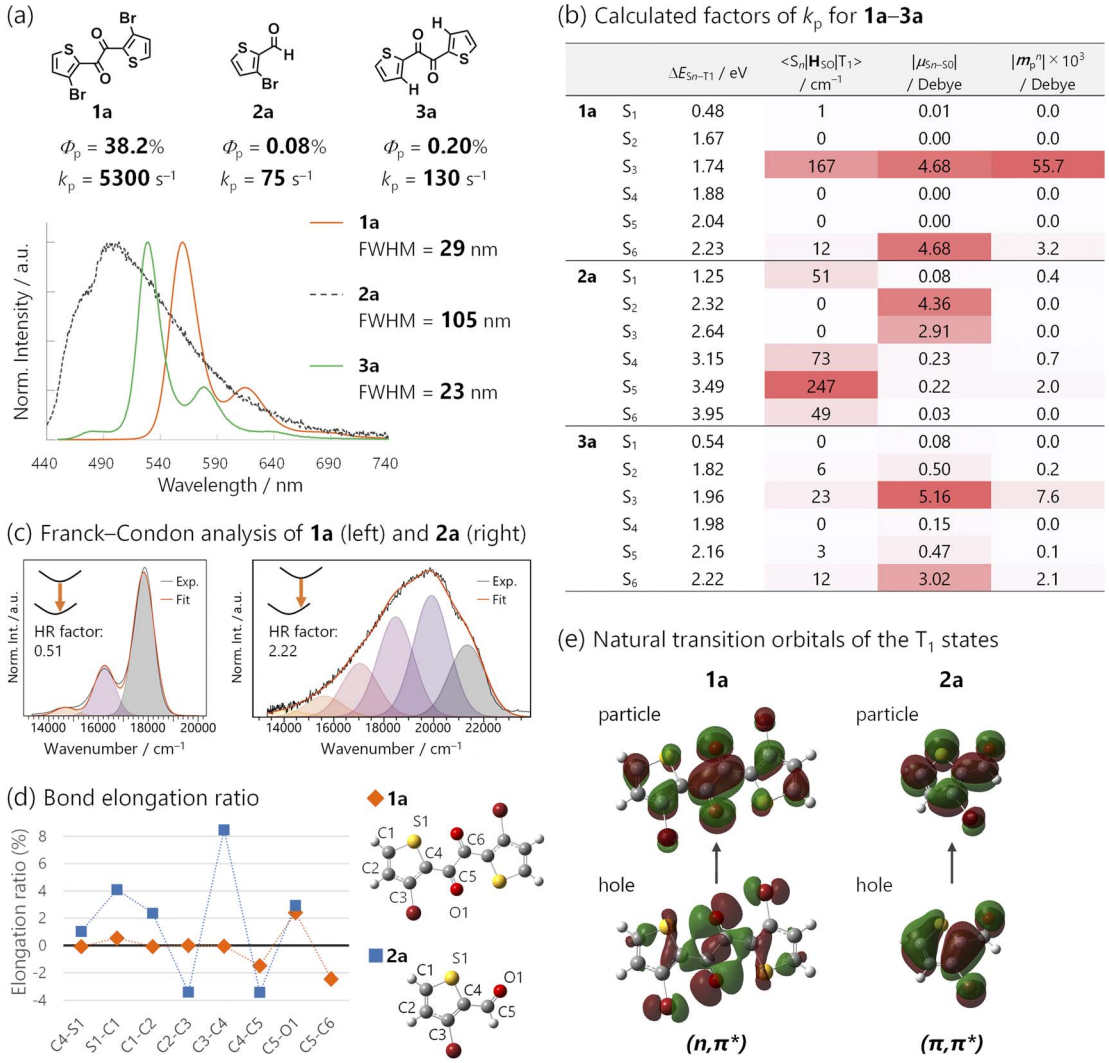

		ΔE_{Sn-T1} / eV	$\langle S_n\|H_{SO}\|T_1\rangle$ / cm^{-1}	$\|\mu_{Sn-S0}\|$ / Debye	$\|m_p^n\| \times 10^3$ / Debye
1a	S_1	0.48	1	0.01	0.0
	S_2	1.67	0	0.00	0.0
	S_3	1.74	167	4.68	55.7
	S_4	1.88	0	0.00	0.0
	S_5	2.04	0	0.00	0.0
	S_6	2.23	12	4.68	3.2
2a	S_1	1.25	51	0.08	0.4
	S_2	2.32	0	4.36	0.0
	S_3	2.64	0	2.91	0.0
	S_4	3.15	73	0.23	0.7
	S_5	3.49	247	0.22	2.0
	S_6	3.95	49	0.03	0.0
3a	S_1	0.54	0	0.08	0.0
	S_2	1.82	6	0.50	0.2
	S_3	1.96	23	5.16	7.6
	S_4	1.98	0	0.15	0.0
	S_5	2.16	3	0.47	0.1
	S_6	2.22	12	3.02	2.1

Fig. 6 (a) Chemical structures of **1a**, **2a**, and **3a**, and their Φ_p, estimated k_p, steady-state photoluminescence spectra, and the corresponding FWHM in cyclohexane (1.0×10^{-5} M, 2.6×10^{-3} M, and 1.0×10^{-4} M, respectively) excited at 368 nm under Ar. k_p was derived as $k_p = \Phi_p/\tau_p$, assuming $\phi_{ISC} = 1$. (b) Calculated factors of k_p for **1a**–**3a**. (c) Franck–Condon analysis of the emission spectra of **1a** (left) and **2a** (right). Huang–Rhys (HR) factors were 0.51 and 2.22, respectively. (d) Bond-elongation ratio between the optimized geometries in the S_0 and T_1 states of **1a** and **2a**. (e) Natural transition orbitals of the T_1 states for **1a** and **2a**.

Structure-RTP property relationship study

The significance of the diketone skeleton for the huge k_p was further evident when comparing **1** with the corresponding bromoaldehyde **2** and diketone without Br atoms **3** (Fig. 6a and b for **1a**, **2a**, and **3a**; Fig. S5† for **1b**, **2b**, and **3b** bearing triisopropylsilyl groups; also see Table S2†). All the compounds exhibited RTP in degassed solutions; however, Φ_p of **1** was much higher than those of **2** and **3** regardless of the silyl substituents (38.2%, 0.08%, and 0.20% for **1a**, **2a**, and **3a**; 24.6%, 0.22%, and 1.2% for **1b**, **2b**, and **3b**, respectively).

The superior Φ_p of **1** was attributed to its large k_p, which was more than one order of magnitude larger than the estimated k_ps of **2** and **3** (Fig. 6a and Table S2†). TDDFT calculations reasonably reproduced this trend; the calculated k_p for **1a**, **2a**, and **3a** was 5400, 9, and 71 s^{-1}, respectively (Fig. S27, S30 and S31†). The small k_p of aldehyde **2** was because of the mismatched $\langle S_n|H_{SO}|T_1\rangle$ and $\mu_{S_n-S_0}$ (Fig. 6b; see Table S4† for **1b**, **2b**, and **3b**). Thus, the T_1 state of **2** had a (π,π*) configuration (Fig. 6e), which coupled strongly to (n,π*) S_n states (*e.g.*, $n = 5$; $\langle S_5|H_{SO}|T_1\rangle$ was as large as 247 cm^{-1} for **2a**). However, the (n,π*) configuration diminishes $\mu_{S_n-S_0}$ (*e.g.*, $|\mu_{S_5-S_0}|$ was only 0.22 *D* for **2a**). Consequently, intensity-borrowing was insufficient, resulting in a small k_p. Hence, a large $\langle S_n|H_{SO}|T_1\rangle$ (or a large mixing coefficient, $\langle S_n|H_{SO}|T_1\rangle/\Delta E_{S_n-T_1}$) itself is insufficient and the combination with a large $\mu_{S_n-S_0}$ in the same *n*-th singlet state is essential for achieving a huge k_p.[31] To meet this requirement, the T_1 state should have a (n,π*) configuration. Indeed, the k_p of Br-free diketone **3a** was larger than that of Br-containing aldehyde **2a**, because the T_1 state of **3a** had a (n,π*) configuration. Thus, the (n,π*) T_1 state prefers coupling with (π,π*) S_n states, whose $\mu_{S_n-S_0}$ can be sizable (*e.g.*, $n = 3$, $|\mu_{S_3-S_0}| = 5.16$ *D* for **3a**; Fig. 6b). However, SOC between these states was not as effective as that for **1a** because of the absence of the heavy atom, Br (*e.g.*, $\langle S_3|H_{SO}|T_1\rangle = 23$ cm^{-1} for **3a**). Therefore, intensity borrowing

was less effective, yielding a lower k_p than the brominated diketone **1a**.

The side-on spatial arrangement of C–Br and C=O was crucial for the heavy-atom effect because of better mutual alignment of the in-plane Br and O p orbitals. This resulted in large hole coefficients in the T_1 state (Fig. 5b).[32] However, the arrangement is energetically unfavourable due to electronic repulsion, because Br and O in the TP geometry of **1** were within the sum of their van der Waals radii according to the X-ray structure (Fig. S32†).[17a,33,34] Indeed, DFT calculations for the aldehyde **2a** indicated that the side-on conformation was less stable (by 3 kcal mol^{-1}) for both S_0 and T_1 states than the conformation with oxygen pointing away from the Br (Fig. S28†).[32] Interestingly, the TP geometry of **1** involved two-fold intramolecular S···O noncovalent chalcogen bonding interactions,[35] with interaction energies as large as 7.74 kcal mol^{-1}, according to the natural bonding orbital analysis of **1a**.[17a] The chalcogen bonds stabilized the TP conformer and increased k_p by forcibly fixing Br in the vicinity of carbonyl oxygens.

Origin of the narrowband emission

Finally, we investigated the origin of the narrowband emission of **1** *via* a comparison of the **1a** emission spectra with those of its aldehyde counterpart, **2a** (Fig. 6a, c–e; see Fig. S18† for the comparison of **1b** with **2b**). Diketones **1a** and **1b** exhibited narrowband emissions (FWHM = 29 and 32 nm) while aldehydes **2a** and **2b** had broadband emissions (FWHM = 105 and 106 nm).

The bandwidths could be strongly correlated with molecular geometry changes in the ground and excited states, which are quantified using the Huang–Rhys (HR) factor obtained from a Franck–Condon analysis of the spectra (Fig. 6c, S18, and Table S3†).[15,36] The HR factor of diketone **1a** (**1b**) was 0.51 (0.50), while that of aldehyde **2a** (**2b**) was 2.22 (2.39). The smaller HR factors in **1** corresponded to smaller geometry changes in the T_1-to-S_0 transition, which were corroborated by DFT calculations. The results indicated that although diketone **1a** and aldehyde **2a** retained their planarity in the transition, bond length changes were small for **1a** and large for **2a**.

We visualized these bond length changes using elongation ratios, defined as $(R_{T1} - R_{S_1})/R_{S_1}$, where R_{T_1} and R_{S_1} represent bond lengths in the T_1-and S_0-optimized geometries; a positive value indicates that the bond is longer in the T_1 state (Fig. 6d). The bond lengths within the thiophene ring of diketone **1a** exhibited minimal changes. Conversely, the absolute values of the elongation ratios were large in the case of aldehyde **2a** (*e.g.*, the bond length between 3C and 4C changed by 8.4%).

These considerable bond length changes in **2a** were attributed to the (π,π^*) character of the T_1 state, as evident in the NTOs (Fig. 6e). The electronic transition from bonding to antibonding orbitals significantly affects the bond strength. In contrast, the NTOs of **1a** were mainly localized on the 1,2-dicarbonyl moiety, and the electronic transition was nonbonding to antibonding, which led to minor changes in the bond lengths (Fig. 6d). Moreover, the transition in the diketones **1** had no net charge-transfer character because of the centrosymmetric geometry. This was in contrast to most aromatic (mono)carbonyl compounds, where $^3(n,\pi^*)$ states have a charge-transfer character from the carbonyl to the aromatic ring. These features of diketones minimized molecular geometry changes during phosphorescence emission. Therefore, the 1,2-diketone-based phosphor would be a promising platform for efficient narrowband RTP.

Conclusions

Efficient narrowband RTP from metal-free organic 3-bromo-2-thienyl diketones was observed in solutions, amorphous polymer matrices, and crystalline solids. A substantial phosphorescence rate constant of ~5000 s^{-1} was experimentally confirmed, which was the key to outstanding RTP quantum yields in solution (38% under Ar) and in polymer films (up to 54% in air). Ultrafast spectroscopy and single-crystal X-ray structure analysis revealed that the fast RTP originated from the diketone planar conformation. Both experimental and theoretical analyses indicated that the planar conformer embodies ideal electronic structures for fast RTP:

1. The planar geometry with a delocalized π-system
2. σ-Symmetric n-orbitals perpendicular to the π-system
3. Heavy atoms conjugated with both π- and n-electron systems
4. (n,π^*) configuration of the T_1 state

Fulfilling these points would be a promising design principle for molecules with large $\boldsymbol{\mu}_{S_n-S_0}$ and $\langle S_n|\mathbf{H}_{SO}|T_1\rangle$ in the same S_n states, and results in a k_p leap. In addition, the centrosymmetric nonbonding-to-antibonding electronic transition of the 1,2-diketone skeleton was the key to the narrowband emission. The fast RTP (large k_p) is potentially advantageous for various applications, such as phosphorescence OLEDs and lasers, triplet-to-singlet conversion *via* Förster resonance energy transfer, bioimaging, and theranostics. However, such applications have been monopolized by precious-metal phosphors. We believe that the mechanistic elucidation paves the way for developing fast organic RTP, which could expand applications of metal-free organic materials.

Data availability

All experimental/computational procedures and data related to this article are provided in the ESI.†

Author contributions

Y. T. project administration: lead; supervision: lead; conceptualisation: equal; funding acquisition: lead; investigation: lead; visualisation: lead; writing—original draft: lead; writing—review & editing: lead. K. M. project administration: lead; supervision: lead; conceptualisation: equal; funding acquisition: lead; investigation: supporting; visualisation: supporting; writing—original draft: supporting; writing—review & editing: lead. E. O., Y. O., M. T., and S. K. investigation: equal. M. K. investigation: equal; funding acquisition: supporting; writing—review & editing: supporting. T. E. and K. K. investigation:

supporting. K. O. and T. O. resources: lead; supervision: supporting.

Conflicts of interest

There are no conflicts to declare.

Acknowledgements

This work was supported by JSPS KAKENHI (grant numbers JP23H03955, JP22H02159, JP20H05676, and JP19K15542). M. K. acknowledges a grant-in-aid for a JSPS Research Fellow (22J12961). Y. T. is grateful to the ENEOS Tonengeneral Research/Development Encouragement & Scholarship Foundation, the Izumi Science and Technology Foundation, the Toyota Physical and Chemical Research Institute, and the Yazaki Memorial Foundation for Science and Technology for the financial support. K. M. acknowledges Sumitomo Basic Science Research Projects, the Kyushu University Q-PIT Support Program for Young Researchers and Doctoral Students, and the Young Researchers Support Project, Faculty of Science, Kyushu University grant numbers 22-A5 (R4). The authors thank Dr Kenich Yamashita (Osaka University) for the lifetime measurements and Dr Yuki Kurashige (Kyoto University) and Dr Ryohei Kishi (Osaka University) for fruitful discussions on the quantum chemical calculations. Computations were performed at the Research Center for Computational Science, Okazaki, Japan (Project: 22-IMS-C153 and 23-IMS-C187). The experiments were partially performed at the Analytical Instrument Facility, Graduate School of Science, Osaka University, using research equipment shared in the MEXT project (JPMXS0441200023).

Notes and references

1 (*a*) S. Hirata, *Adv. Opt. Mater.*, 2017, **5**, 1700116; (*b*) Kenry, C. Chen and B. Liu, *Nat. Commun.*, 2019, **10**, 2111.

2 (*a*) P.-T. Chou and Y. Chi, *Chem.–Eur. J.*, 2007, **13**, 380–395; (*b*) Q. Zhao, C. Huang and F. Li, *Chem. Soc. Rev.*, 2011, **40**, 2508–2524; (*c*) C. Fan and C. Yang, *Chem. Soc. Rev.*, 2014, **43**, 6439–6469; (*d*) C.-P. Tan, Y.-M. Zhong, L.-N. Ji and Z.-W. Mao, *Chem. Sci.*, 2021, **12**, 2357–2367.

3 (*a*) A. Bouskila, B. Drahi, E. Amouyal, I. Sasaki and A. Gaudemer, *J. Photochem. Photobiol., A*, 2004, **163**, 381–388; (*b*) A. K. Bansal, W. Holzer, A. Penzkofer and T. Tsuboi, *Chem. Phys.*, 2006, **330**, 118–129; (*c*) A. Endo, K. Suzuki, T. Yoshihara, S. Tobita, M. Yahiro and C. Adachi, *Chem. Phys. Lett.*, 2008, **460**, 155–157; (*d*) J. R. Sommer, A. H. Shelton, A. Parthasarathy, I. Ghiviriga, J. R. Reynolds and K. S. Schanze, *Chem. Mater.*, 2011, **23**, 5296–5304.

4 (*a*) N. J. Turro, V. Ramamurthy and J. C. Scaiano, *Principles of Molecular Photochemistry: An Introduction*, University Science Books, Sausalito, CA, 2009; (*b*) N. S. e. Konstantin and A. B. Elena, *Phys.-Usp.*, 2005, **48**, 231; (*c*) M. Kasha, *J. Chem. Phys.*, 1952, **20**, 71–74; (*d*) D. S. McClure, *J. Chem. Phys.*, 1949, **17**, 905–913; (*e*) D. R. Kearns and W. A. Case, *J. Am. Chem. Soc.*, 1966, **88**, 5087–5097.

5 (*a*) J. J. Donkerbroek, J. J. Elzas, C. Gooijer, R. W. Frei and N. H. Velthorst, *Talanta*, 1981, **28**, 717–723; (*b*) J. Xu, A. Takai, Y. Kobayashi and M. Takeuchi, *Chem. Commun.*, 2013, **49**, 8447–8449; (*c*) B. Ventura, A. Bertocco, D. Braga, L. Catalano, S. d'Agostino, F. Grepioni and P. Taddei, *J. Phys. Chem. C*, 2014, **118**, 18646–18658; (*d*) G. D. Gutierrez, G. T. Sazama, T. Wu, M. A. Baldo and T. M. Swager, *J. Org. Chem.*, 2016, **81**, 4789–4796; (*e*) Z. Yu, Y. Wu, L. Xiao, J. Chen, Q. Liao, J. Yao and H. Fu, *J. Am. Chem. Soc.*, 2017, **139**, 6376–6381; (*f*) H. Shu, H. Li, J. Rao, L. Chen, X. Wang, X. Wu, H. Tian, H. Tong and L. Wang, *J. Mater. Chem. C*, 2020, **8**, 14360–14364.

6 (*a*) A. Maciejewski and R. P. Steer, *Chem. Rev.*, 1993, **93**, 67–98; (*b*) M. Szymanski, R. P. Steer and A. Maciejewski, *Chem. Phys. Lett.*, 1987, **135**, 243–248; (*c*) M. Szymanski, A. Maciejewski and R. P. Steer, *J. Phys. Chem.*, 1988, **92**, 2485–2489.

7 J. D. Coyle, *Tetrahedron*, 1985, **41**, 5393–5425.

8 (*a*) A. Forni, E. Lucenti, C. Botta and E. Cariati, *J. Mater. Chem. C*, 2018, **6**, 4603–4626; (*b*) W. Zhao, Z. He and B. Z. Tang, *Nat. Rev. Mater.*, 2020, **5**, 869–885; (*c*) A. D. Nidhankar, Goudappagouda, V. C. Wakchaure and S. S. Babu, *Chem. Sci.*, 2021, **12**, 4216–4236.

9 (*a*) D. B. Clapp, *J. Am. Chem. Soc.*, 1939, **61**, 523–524; (*b*) W. Z. Yuan, X. Y. Shen, H. Zhao, J. W. Y. Lam, L. Tang, P. Lu, C. Wang, Y. Liu, Z. Wang, Q. Zheng, J. Z. Sun, Y. Ma and B. Z. Tang, *J. Phys. Chem. C*, 2010, **114**, 6090–6099; (*c*) O. Bolton, K. Lee, H. J. Kim, K. Y. Lin and J. Kim, *Nat. Chem.*, 2011, **3**, 205–210; (*d*) M. Shimizu, R. Shigitani, M. Nakatani, K. Kuwabara, Y. Miyake, K. Tajima, H. Sakai and T. Hasobe, *J. Phys. Chem. C*, 2016, **120**, 11631–11639; (*e*) E. Hamzehpoor and D. F. Perepichka, *Angew. Chem., Int. Ed.*, 2020, **59**, 9977–9981; (*f*) A. Fermi, G. Bergamini, R. Peresutti, E. Marchi, M. Roy, P. Ceroni and M. Gingras, *Dyes Pigm.*, 2014, **110**, 113–122; (*g*) Y. Wen, H. Liu, S. Zhang, Y. Gao, Y. Yan and B. Yang, *J. Mater. Chem. C*, 2019, **7**, 12502–12508.

10 (*a*) S. Hirata, K. Totani, J. Zhang, T. Yamashita, H. Kaji, S. R. Marder, T. Watanabe and C. Adachi, *Adv. Funct. Mater.*, 2013, **23**, 3386–3397; (*b*) M. S. Kwon, Y. Yu, C. Coburn, A. W. Phillips, K. Chung, A. Shanker, J. Jung, G. Kim, K. Pipe, S. R. Forrest, J. H. Youk, J. Gierschner and J. Kim, *Nat. Commun.*, 2015, **6**, 8947; (*c*) M. S. Kwon, D. Lee, S. Seo, J. Jung and J. Kim, *Angew. Chem., Int. Ed.*, 2014, **53**, 11177–11181; (*d*) Y. Su, S. Z. F. Phua, Y. Li, X. Zhou, D. Jana, G. Liu, W. Q. Lim, W. K. Ong, C. Yang and Y. Zhao, *Sci. Adv.*, 2018, **4**, eaas9732; (*e*) H. Wu, W. Chi, Z. Chen, G. Liu, L. Gu, A. K. Bindra, G. Yang, X. Liu and Y. Zhao, *Adv. Funct. Mater.*, 2019, **29**, 1807243; (*f*) Z.-Y. Zhang, W.-W. Xu, W.-S. Xu, J. Niu, X.-H. Sun and Y. Liu, *Angew. Chem., Int. Ed.*, 2020, **59**, 18748–18754.

11 W. Shao and J. Kim, *Acc. Chem. Res.*, 2022, **55**, 1573–1585.

12 (*a*) Z. Zhou, X. Xie, Z. Sun, X. Wang, Z. An and W. Huang, *J. Mater. Chem. C*, 2023, **11**, 3143–3161; (*b*) H. Imahori, Y. Kobori and H. Kaji, *Acc. Mater. Res.*, 2021, **2**, 501–514.

13 W. Shao, H. Jiang, R. Ansari, P. M. Zimmerman and J. Kim, *Chem. Sci.*, 2022, **13**, 789–797.

14 I. Partanen, O. Al-Saedy, T. Eskelinen, A. J. Karttunen, J. J. Saarinen, O. Mrózek, A. Steffen, A. Belyaev, P.-T. Chou and I. O. Koshevoy, *Angew. Chem., Int. Ed.*, 2023, **62**, e202305108.

15 J. M. Ha, S. H. Hur, A. Pathak, J.-E. Jeong and H. Y. Woo, *NPG Asia Mater.*, 2021, **13**, 53.

16 (*a*) H. L. J. Bäckström and K. Sandros, *Acta Chem. Scand.*, 1960, **14**, 48–62; (*b*) D. J. Morantz and A. J. C. Wright, *J. Chem. Phys.*, 1971, **54**, 692–697; (*c*) L. Flamigni, F. Barigelletti, S. Dellonte and G. Orlandi, *J. Photochem.*, 1983, **21**, 237–244; (*d*) A. K. Singh, D. K. Palit and J. P. Mittal, *Chem. Phys. Lett.*, 2002, **360**, 443–452; (*e*) Y. Tsuboi, K. Okada, S. Ishizaka and N. Kitamura, *Anal. Sci.*, 2005, **21**, 303–308; (*f*) Y. Gong, Y. Tan, H. Li, Y. Zhang, W. Yuan, Y. Zhang, J. Sun and B. Z. Tang, *Sci. China: Chem.*, 2013, **56**, 1183–1186.

17 (*a*) Y. Tani, M. Terasaki, M. Komura and T. Ogawa, *J. Mater. Chem. C*, 2019, **7**, 11926–11931; (*b*) Y. Tani, M. Komura and T. Ogawa, *Chem. Commun.*, 2020, **56**, 6810–6813; (*c*) Y. Takewaki, T. Ogawa and Y. Tani, *Front. Chem.*, 2022, **9**, 812593.

18 M. Komura, T. Ogawa and Y. Tani, *Chem. Sci.*, 2021, **12**, 14363–14368.

19 M. Komura, H. Sotome, H. Miyasaka, T. Ogawa and Y. Tani, *Chem. Sci.*, 2023, **14**, 5302–5308.

20 Vibronic band is a term for the band due to the transition from the vibrational ground state of an electronic excited state to different vibrational levels of the S_0 (electronic ground) state. We have confirmed this assignment by TRPL measurements, where the whole spectrum decayed at the same rate (Fig. S12†).

21 In 2014, a family of organic boron complexes was reported to show RTP in solution with a quantum yield over 100% due to singlet fission. However, in 2022, another group evidently pointed out that the RTP was an artifact. They mentioned that "it is obvious that the error is caused by the limit of the dynamic range of the instrument," and that the compound "exhibits solely a highly intense fluorescence in CH_2Cl_2 with no indication of phosphoresce and dual emission in the room temperature solution." See ref. 22 for details.

22 (*a*) M. Koch, K. Perumal, O. Blacque, J. A. Garg, R. Saiganesh, S. Kabilan, K. K. Balasubramanian and K. Venkatesan, *Angew. Chem., Int. Ed.*, 2014, **53**, 6378–6382; (*b*) Y. Chen, C.-H. Wang, T.-C. Chou and P.-T. Chou, *Angew. Chem., Int. Ed.*, 2022, **61**, e202109224.

23 During the review process of this manuscript, X. Peng *et al.* published a report on an efficient organic RTP in solution. The total photoluminescence quantum yield (PLQY) in toluene was reported to be as high as 60% under N_2 and 8% under O_2; however, neither the RTP QY nor the intersystem crossing efficiency was investigated, and the RTP rate constant remains unclear. According to the reported fluorescence lifetimes and PL decay curve, total PLQY under N_2 should include a considerable fluorescence contribution. These results highlight the significance of evaluating the intersystem crossing efficiency. See: X. Peng, P. Zou, J. Zeng, X. Wu, D. Xie, Y. Fu, D. Yang, D. Ma, B. Z. Tang and Z. Zhao, *Angew. Chem., Int. Ed.*, 2024, **63**, e202405418.

24 (*a*) T. Nakashima, M. Shimada, Y. Kurihara, M. Tsuchiya, Y. Yamanoi, E. Nishibori, K. Sugimoto and H. Nishihara, *J. Organomet. Chem.*, 2016, **805**, 27–33; (*b*) M. Shimizu, T. Kinoshita, R. Shigitani, Y. Miyake and K. Tajima, *Mater. Chem. Front.*, 2018, **2**, 347–354; (*c*) S. Hirata, *Adv. Sci.*, 2019, **6**, 1900410; (*d*) M. Shimizu, S. Nagano and T. Kinoshita, *Chem.–Eur. J.*, 2020, **26**, 5162–5167.

25 N. Gan, H. Shi, Z. An and W. Huang, *Adv. Funct. Mater.*, 2018, **28**, 1802657.

26 D. Lee, O. Bolton, B. C. Kim, J. H. Youk, S. Takayama and J. Kim, *J. Am. Chem. Soc.*, 2013, **135**, 6325–6329.

27 (*a*) Z. He, W. Li, G. Chen, Y. Zhang and W.-Z. Yuan, *Chin. Chem. Lett.*, 2019, **30**, 933–936; (*b*) J. Song, L. Ma, S. Sun, H. Tian and X. Ma, *Angew. Chem., Int. Ed.*, 2022, **61**, e202206157; (*c*) M. Yasui, T. Fujihara, H. Ohtsu, Y. Wada, T. Shimada, Y. Zhu, M. Kawano, K. Hanaya, T. Sugai and S. Higashibayashi, *Commun. Chem.*, 2023, **6**, 245; (*d*) Z. Chen, X. Chen, D. Ma, Z. Mao, J. Zhao and Z. Chi, *J. Am. Chem. Soc.*, 2023, **145**, 16748–16759; (*e*) S. H. Lee, M. S. Valverde Paredes, P. M. Forster and D.-C. Lee, *RSC Adv.*, 2024, **14**, 6285–6291.

28 (*a*) G. Baryshnikov, B. Minaev and H. Ågren, *Chem. Rev.*, 2017, **117**, 6500–6537; (*b*) T. J. Penfold, E. Gindensperger, C. Daniel and C. M. Marian, *Chem. Rev.*, 2018, **118**, 6975–7025.

29 M. J. G. Peach and D. J. Tozer, *J. Phys. Chem. A*, 2012, **116**, 9783–9789.

30 H. Ma, Q. Peng, Z. An, W. Huang and Z. Shuai, *J. Am. Chem. Soc.*, 2019, **141**, 1010–1015.

31 (*a*) S. Hirata, *J. Phys. Chem. Lett.*, 2018, **9**, 4251–4259; (*b*) I. Bhattacharjee and S. Hirata, *Adv. Mater.*, 2020, **32**, 2001348.

32 S. Sarkar, H. P. Hendrickson, D. Lee, F. DeVine, J. Jung, E. Geva, J. Kim and B. D. Dunietz, *J. Phys. Chem. C*, 2017, **121**, 3771–3777.

33 One might expect the formation of halogen bonding (attractive interactions) in side-on arrangements. However, it is unlikely because the halogen bonding is a highly directional interaction between the lone pair of (in this case) carbonyl O and "sigma-hole" of Br that forms along the C–Br σ* bond. Indeed, there were no donor–acceptor interactions found between Br···O according to natural bonding orbital analysis of **1a**.

34 S. J. Ang, T. S. Chwee and M. W. Wong, *J. Phys. Chem. C*, 2018, **122**, 12441–12447.

35 (*a*) D. J. Pascoe, K. B. Ling and S. L. Cockroft, *J. Am. Chem. Soc.*, 2017, **139**, 15160–15167; (*b*) H. Huang, L. Yang, A. Facchetti and T. J. Marks, *Chem. Rev.*, 2017, **117**, 10291–10318; (*c*) R. Gleiter, G. Haberhauer, D. B. Werz, F. Rominger and C. Bleiholder, *Chem. Rev.*, 2018, **118**, 2010–2041.

36 M. de Jong, L. Seijo, A. Meijerink and F. T. Rabouw, *Phys. Chem. Chem. Phys.*, 2015, **17**, 16959–16969.